Author Manuscript

Author Manuscript

Author Manuscript

Author Manuscript

HHS Public Access

Author manuscript

Clin Cancer Res. Author manuscript; available in PMC 2023 March 15.

Acetylated HOXB13 Regulated Super Enhancer Genes Define Therapeutic Vulnerabilities of Castration-Resistant Prostate Cancer

Duy T. Nguyen[1,2,4,#], **Wei Yang**[3,#], **Arun Renganathan**[1,2], **Cody Weimholt**[5], **Duminduni H. Angappulige**[1,2], **Thanh Nguyen**[1,2,6], **Robert W. Sprung**[7], **Gerald L. Andriole**[1,2,8,9], **Eric H. Kim**[1,2,9], **Nupam P. Mahajan**[1,2,9], **Kiran Mahajan**[1,2,9,#,*]

[1]Division of Urologic Surgery, Washington University in St. Louis, St. Louis, MO, 63110, USA.

[2]Department of Surgery, Washington University in St. Louis, St. Louis, MO, 63110, USA.

[3]Genome Technology Access Center, Department of Genetics, Washington University in St. Louis, St. Louis, MO, 63110, USA.

[4]Mayo Clinic Graduate School of Biomedical Science, College of Medicine & Science, Rochester, MN, 55905, USA.

[5]Department of Pathology and Immunology, Washington University in St. Louis, St. Louis, MO, 63110, USA.

[6]Cancer and Cell Biology Graduate Program, Baylor College of Medicine, Houston, TX 77030, USA.

[7]Division of Endocrinology, Metabolism and Lipid Research, Washington University School of Medicine, St. Louis, MO, 63110, USA.

[8]National Capital Region, Johns Hopkins Medicine, Sibley Memorial Hospital, Washington DC 20016, USA.

[9]Siteman Cancer Center, Washington University in St. Louis, St. Louis, MO, 63110, USA.

Abstract

Purpose: Androgen Receptor (AR) antagonism is exacerbated by HOXB13 in Castration Resistant Prostate Cancers (CRPCs). However, it is unclear when and how does HOXB13 prime CRPCs for AR antagonism. By mass-spectrometry analysis of CRPC extract we uncovered a novel

[*]**Corresponding author:** Kiran Mahajan, PhD, Assistant Professor of Surgery, Campus Box 8242, 660 South Euclid Avenue, Washington University in St. Louis, St. Louis, MO 63110-1093, Tel no: 314-273-7728, kiranm@wustl.edu.
[#]Equal contribution

Author contributions

K.M. conceived, designed, supervised the study and wrote the manuscript. D.N. K.M., AR. D.H.A and T.N performed the experiments. W.Y. conducted the bioinformatic analysis. C.W. performed pathology review of histological and IHC sections. E.H.K. and G. L. A. provided prostate tissue specimens. N.P.M provided ACK1 inhibitor. R.W.S. supervised proteomic analysis. K.M, D.N, W.Y, A.R. and R.W.S compiled the methodology. All authors reviewed and approved the manuscript.

Competing interests' statements

K.M. and N.P.M. are co-founders of Technogenesys, a startup company that controls the intellectual property and patents on the ACK1 inhibitor (R)-9b. All other authors have no conflicts of interest to declare. Washington University has filed for a patent for the use of acetylated HOXB13 antibodies for the detection of clinically significant prostate cancer.

Author Manuscript Author Manuscript Author Manuscript Author Manuscript

lysine 13 (K13) acetylation in HOXB13 mediated by CBP/p300. To determine whether acetylated K13-HOXB13 is a clinical biomarker of CRPC development, we characterized its role in prostate cancer biology.

Experimental Design: We identified tumor-specific acK13-HOXB13 signal enriched Super enhancer (SE) regulated targets. We analyzed the effect of loss of HOXB13K13-acetylation on chromatin binding, SE proximal target gene expression, self-renewal, enzalutamide sensitivity and CRPC tumor growth employing isogenic parental and *HOXB13K13A* mutants. Finally, using primary human prostate organoids we evaluated whether inhibiting an acK13-HOXB13 target, ACK1, with a selective inhibitor (R)-9b is superior to AR antagonists in inhibiting CRPC growth.

Results: acK13-HOXB13 promotes increased expression of lineage (*AR, HOXB13*), PC diagnostic (*FOLH1*) CRPC-promoting (*ACK1*) and angiogenesis (*VEGFA, Angiopoietins*) genes early in PC development by establishing tumor-specific SEs. acK13-HOXB13 recruitment to key SE regulated targets is insensitive to Enzalutamide. ACK1 expression is significantly reduced in the loss of function *HOXB13K13A* mutant CRPCs. Consequently, *HOXB13K13A* mutants display reduced self-renewal, increased sensitivity to enzalutamide and impaired xenograft tumor growth. Primary human prostate tumor organoids expressing HOXB13 are significantly resistant to AR antagonists but sensitive to (R)-9b.

Conclusions: In summary, acetylated HOXB13 is a biomarker of clinically significant PC. Importantly, PSMA-targeting agents and (R)-9b could be new therapeutic modalities to target HOXB13-ACK1 axis regulated PCs.

Keywords

Prostate Cancer; HOXB13; p300/CBP; lysine acetylation; super-enhancers; androgen receptor; castration-resistance; angiopoietins; epigenetics; ACK1; (R)-9b; *FOLH1* ; PSMA

Introduction

PC afflicts ~1.3 million men worldwide and is a leading cause of global cancer-related deaths (1). Patients diagnosed with hormone-sensitive PC who undergo treatment with androgen deprivation therapy (ADT) invariably develop CRPC (2–4). Following disruption of the primary androgen-androgen receptor (AR)-mediated regulatory axis, cancer cells activate bypass mechanisms for survival (5,6). Notably, cancer cells that activate pioneer transcription factor (TF) regulated programs appear not only tolerate hormone deprivation better but are also characterized by an increased metastatic potential (7–12). The mechanism by which developmental TFs direct prostatic luminal epithelial cells away from differentiation is currently unclear.

Epigenetic deregulation of developmentally regulated chromatin readers and pioneer transcription factors co-ordinates reactivation of quiescent gene expression programs to transform cells permanently into new subtypes (13–15). However, tissue-specific TFs may themselves function as epigenetic regulators during this cellular transformation. Identifying this *de novo* epigenetic activity of TF is critical to understand their role in overcoming the programming of normal cells for differentiation. Pioneer TFs, HOXB13 and FOXA1, regulate prostate differentiation through their interactions with the AR and enhancers,

Author Manuscript Author Manuscript Author Manuscript Author Manuscript

largely under the influence of testosterone (16–19). Particularly, the HOXB13 Glycine 84 to Glutamic acid (G84E) mutation is associated with an increased risk for PC (20). Moreover, increased expression of HOXB13 correlates with biochemical recurrence and metastatic progression after radical prostatectomy and promotes resistance to ADT (18,21–23). Whether HOXB13 functions as an epigenetic regulator of prostate cellular transformation to the malignant CRPC state is unknown.

Acetylation of histone and non-histone proteins is known to play a major role in eukaryotic transcriptional regulation (24,25). While enhancers and Super-Enhancer (SE)-regulated transcriptional networks are emerging features in many tumor types (26,27), how cells mark pathogenic SEs in the genome is unclear. In this study, we identified K13-acetylated (acK13)-HOXB13 mediated by the histone acetyl transferase CBP/p300 as a critical regulator of SE selectivity prior to CRPC development. We uncovered that acK13-HOXB13 synergizes with H3K27 acetylation at lineage-specific and tumor-promoting SEs of critical CRPC targets, thereby functioning as an epigenetic regulator of tumor growth. Our studies indicate prior treatment with a selective-kinase inhibitor (R)-9b may prevent the establishment of the lethal CRPC state by eliminating cells primed for castration resistance.

Materials and Methods

Cell lines and generation of *HOXB13K13A* mutants

RWPE-1, LNCaP, VCaP, PC-3, 22Rv1 and HEK293T were obtained from American Type Culture Collection. C4-2B and LAPC4 were cultured as described previously (28). All cell lines were used within 3 months or 6–8 passages before being replenished from frozen stocks. The *HOXB13K13A* site-directed mutant C4–2B and 22Rv1 clones described in this study were generated by the Genome Engineering and iPSC Center (GEIC core) at the Washington University in St. Louis. Single-cell clones were verified for nucleotide substitution and single nucleotide polymorphisms by DNA sequencing. All cultures were tested for mycoplasma contamination every 2 months using the PCR Mycoplasma Test Kit I/C (PromoKine). Identities of all cell lines were confirmed by Short Tandem Repeat (STR) Profiling.

Recombinant HOXB13-WT and K13 acetylation mutant constructs

HA-tagged or GFP-tagged full-length HOXB13, HOXB13-K13A, HOXB13-K13R and HOXB13-G84E constructs were generated by Genscript and verified by sequencing. Flag-tagged CBP, His-tagged p300, and additional Flag-tagged HATs (GCN5, TIP60) and GFP-TAF1 were purchased from Addgene.

Generation of HOXB13- K13 acetylation specific monoclonal and polyclonal antibodies

Biotinylated modified and unmodified HOXB13 peptides were synthesized by Genscript. High-titer rabbit polyclonal antibodies directed against acetylated HOXB13-K13 were generated by Genscript and affinity-purified. Monoclonal antibody targeting acetylated HOXB13 were generated by ProMab. acK13-HOXB13-specific antibodies were screened by ELISA against the modified and unmodified HOXB13-K13 peptides. Hybridoma

Author Manuscript Author Manuscript Author Manuscript Author Manuscript

supernatants from the 2B7C1 clone were purified using the Capturem Protein G Maxiprep Columns (Takara Bio USA).

Antibodies

pan-HOXB13 (F-9) monoclonal, SCBT Cat#sc-28333 (RRID: AB_627744), pan-HOXB13 (H-80) polyclonal, SCBT Cat#sc-66923 (RRID: AB_2233136), pan-HOXB13 (D7N8O) CST Cat#90944 (RRID: AB_2734734), AR (F39.4.1), BioGenex Cat#AM256 (RRID: AB_2687514), CBP (D6C5) CST, Cat#7389 (RRID: AB_2616020); p300 (F-4) SCBT Cat# sc-48343 (RRID: AB_ 628075); CTCF Diagenode Cat#C15410210 (RRID: AB_2753160); Total H3 (96C10) CST Cat#3638 (RRID: AB_1642229); H3K27ac CST Cat#4353 (RRID-AB_10949503); H3K27ac Active Motif Cat#39133 (RRID: AB_2561016); Total H4 (L64C1) CST, Cat#2935 (RRID: AB_1147658); H4 pan-acetyl; Active Motif, Cat#39925 (RRID: AB_2687872); HA (C29F4), CST Cat#3724 (RRID: AB_1549585); FLAG (M2); Sigma-Aldrich Cat#F1804 (RRID: AB_262044); Histidine (RM146); Sigma-Aldrich; Cat#SAB5600227 (RRID: AB_2810125); β-Actin (AC-74); Sigma-Aldrich Cat#A2228; (RRID: AB_476697); BRD9, Bethyl laboratories (A303-781A) RRID: AB_11218396; HRP-conjugated anti-mouse; Promega Cat#W4021 (RRID: AB_430834); HRP-conjugated anti-rabbit; Promega Cat#W4011 (RRID: AB_430833).

Cell transfection

C4-2B cells were transfected with siRNAs using the Nucleofector Kit R from Lonza. Plasmid or siRNA transfection was performed on 22Rv1, VCaP, LAPC4 and HEK293T cells using the X-tremeGENE transfection reagent (Sigma). Transfected cells were harvested for analysis after 2 days. siRNAs and primer sequences are provided in Supplementary data.

Co-immunoprecipitation Experiments

Co-immunoprecipitation was performed as described earlier (28) or with Capturem beads from Takara Bio. Cells were sonicated in RLB buffer containing 250–500 mM NaCl (28). Protein extracts (0.5–1 mg) were immunoprecipitated using an anti-HA affinity gel or 3–4 μg of antibody directed against pan- or K13ac-HOXB13 coupled to protein A/G agarose beads. After overnight incubation, the beads were washed with RLB and 1X phosphate-buffered saline (PBS), boiled in sample buffer, electrophoresed (SDS-PAGE) and immunoblotted with the respective antibodies.

Chromatin immunoprecipitation analysis

ChIP-IT Express or ChIP-IT High Sensitivity kit (Active Motif) were used for Chromatin immunoprecipitation experiment. Fresh human prostate tissue specimens were minced while on dry ice and fixed immediately with 1% formaldehyde for 10 minutes. Cell lines were grown in charcoal stripped medium for 48 hours prior to crosslinking with 1% formaldehyde upon reaching 70–80% confluency. DNA was purified using a PCR purification kit (Qiagen) followed by analysis by quantitative PCR or high-throughput sequencing. To identify the maximum number of HOXB13 acetylation binding sites from ChIP-sequencing, we used a HiSeq 3000 sequencing system which results in ~350 million reads per lane at a 1 × 50 read

Author Manuscript Author Manuscript Author Manuscript Author Manuscript

length. The DNA sequencing data were processed using a pipeline that was generated for use in the Encyclopedia of DNA Elements (ENCODE) project.

Peptide pull-down assay to uncover acK13-HOXB13-interacting proteins

Two human HOXB13 peptides (amino acids 1–25) were synthesized with K13 at the center as shown below. Both the peptides were biotinylated at N-terminus. Peptide sequences are as follows:

Unmodified HOXB13 (1–25): NH_2-MEPGNYATLDGA**K**DIEGLLGAGGGR-COOH

K13ac-HOXB13 (1–25): NH_2-MEPGNYATLDGA**K(ac)**DIEGLLGAGGGR-COOH

The biotinylated peptides were immobilized on streptavidin-coupled magnetic beads for 30 minutes at room temperature. After several washes, the peptide-bound beads were incubated with pre-cleared cell lysates in IP-mass spectrometry (MS)-compatible cell lysis buffer (Pierce Cat # 90409) at 4°C overnight. After extensive washing, the captured peptide/protein complexes were isolated via an on-bead digestion method, and nano-LC MS/MS was performed. Competition experiments were performed with acetylated histone H4K5ac peptide; SGRG-Lys-Ac-GGKGLGKGGA.

Cell proliferation Assay

Cells were seeded in 96-well plates containing 200 μl of growth medium per well. Eight replicates were included for each concentration. Four days after the addition of the drug, 25 μl of cell titer-Glo 2.0 (Promega) was added to each well, and luminescence was recorded after 15 minutes using a Synergy HTX multi-mode reader (BioTek). The half-maximal inhibitory concentrations (IC_{50}) were calculated using GraphPad Prism version 8.4.3.

Colony Formation assay

For colony-forming unit (CFU) assay, parental or *HOXB13K13A* mutant C4-2B or 22Rv1 single cells were plated in six-well plates in 3 replicates and cultured for 2 weeks in C4-2B medium or for 22Rv1 in charcoal stripped medium, respectively. Cells were fixed with 4% crystal violet solution in 1% methanol and 4% paraformaldehyde solution. Macroscopic colonies visible were counted using Image J and the area of individual colonies was plotted using Graph Pad Prism version 8.4.3.

Spheroid assay

Parental and *HOXB13K13A* mutant cells (C4-2B or 22Rv1) were seeded in a 24-well plate at approximately 5000 cells per well in 40 μl of growth factor-reduced and phenol red-free Matrigel medium (Corning CB-40234) and maintained in organoid culture medium. 3D-images were captured on an EVOS M5000 microscope (Invitrogen) and analyzed using ImageJ.

Xenograft tumor studies

All animal studies were performed under approved Institutional Animal Care and Use Committee protocols at Washington University in St. Louis. Mice were randomized prior

Author Manuscript Author Manuscript Author Manuscript Author Manuscript

to the injection of the cells. Two million C4-2B cells (parental or *HOXB13K13A* mutants) in 200 ul of growth media in 50% Matrigel (Corning) were implanted subcutaneously into the dorsal flanks of 6-week-old male SCID mice (Charles River Laboratories; n=6 to 8 mice per group). Tumor growth was monitored over a 10-week period. Tumor volumes were measured twice weekly using calipers. At the end of the study, all mice were euthanized humanely. Xenograft tumors were harvested, weighed, and photographed and obtained after euthanasia.

Human prostate tissue studies

Prostate tissues (fresh or formalin fixed) were collected after obtaining informed written consent from prostate cancer patients and the studies were conducted in accordance with the recognized ethical guidelines pertaining to the Declaration of Helsinki after approval by the Institutional Review Board at the Washington University in St. Louis (IRB) (HRPO #201411135; 202010061). The patients were men at 50–75 years of age. Each of the normal and tumor specimens (~3 mm) were obtained fresh post radical prostatectomy, based on MRI-guided biopsy collection and pathology report. A board-certified GU pathologist reviewed ~0.5 to 1 mm hematoxylin and eosin-stained (H and E) stained-FFPE specimens from each case to confirm tumor cellularity. Supplementary Table S1 and Supplementary Figure S3 include clinical annotation for all the specimens used in this study.

Processing of human prostate tumor tissue for organoid generation

Freshly isolated prostate tissues were placed in sterile 60 mm dishes, washed twice with PBS, and minced into ~0.1–0.5 mm pieces. Minced tissues were transferred into 2 ml of cell dissociation media containing collagenase (29) and incubated at 37 °C for 45 min to 1 hr with continuous gentle rotation. The dissociated prostate tissues were centrifuged at 500 × *g* for 5 minutes at 4 °C. The tissues were dissociated further with 5 ml of TrypLE enzymes (Gibco, no. 12605–028) with Rho-associated, coiled-coil containing protein kinase (ROCK) inhibitor (Y27632) for 20 minutes. Approximately 10 ml of ice-cold human prostate organoid culture media was added followed by centrifugation at 500 × *g* for 5 minutes at 4 °C. The dissociated cell suspension was again filtered through a 40-μm mesh filter. Cells were resuspended in 75% Matrigel plus organoid culture media and plated in a single 40 μl drop in the middle of a well in a 24-well plate to create a dome shape. The plate was inverted and incubated for 30 min at 37°C and 5% CO_2. Complete human prostate organoids culture medium (0.5 ml) was added after the matrigel had solidified. Cultures were maintained until organoids (PDOs) reached 300-microns in size. Medium was replenished every 3–4 days to maintain the integrity of PDOs. Organoid images were captured using an EVOS M5000 microscope (Invitrogen) and analyzed using ImageJ or Adobe Photoshop.

Prostate organoid viability assay

Prostate organoids were grown in matrigel domes in a 24-well plate with 600 μl organoid culture medium and treated with vehicle or inhibitor. After 6 days, media was withdrawn, cells were recovered by incubating in 200 μl of cell recovery solution (Corning 354253) at 4°C on a rotator for 60 min. 50 μl of CellTiter-Glo 2.0 (Promega) was added to each well and the contents were transferred to a 96 well-microtiter plate. Luminescence was

Author Manuscript Author Manuscript Author Manuscript Author Manuscript

recorded after 15 minutes using a Synergy HTX multi-mode reader (BioTek). Percent cell viability was calculated by normalizing the readings obtained in response to each inhibitor concentration to the readings in vehicle (DMSO).

Single cell RNA sequencing and transcriptomic analysis

Single-cell suspensions from 6750 cells were generated from prostate tissue organoids for library preparation as described in the 10X Genomics single-cell suspension protocol. All RNA samples were quantitated twice on the bioanalyzer and checked to ensure integrity. Sequencing was performed at 25K depth per cell using the NovaSeq S4 flow cell. Cell Ranger software was used to align the reads to genome reference GRCh38. Loupe browser analysis was performed to generate t-SNE plots.

Statistical Analysis

All data are presented as means ± standard error of the mean (SEM). Statistical analyses included unpaired Student's t-test to compare two groups; analysis of variance (ANOVA) was used for three or more group comparison by GraphPad Prism software. All p values <0.05 were considered to be statistically significant.

Resource availability

HOXB13-K13 acetylation antibodies, C4-2B and 22Rv1 *HOXB13K13A* mutants, reagents and recombinant DNA constructs will be made available upon request to Dr. Kiran Mahajan. kiranm@wustl.edu.

Data availability

GSE167506, GSE169134, GSE169132, GSE169133. Human prostate ChIP-sequencing data is maintained in WashU server and will be provided upon request.

Results

p300/CBP mediated HOXB13 acetylation at lysine 13 is androgen receptor-independent

To investigate the mechanism by which HOXB13 promotes lethal prostate cancer, we affinity-purified HOXB13 from the metastatic CRPC cell line, C4-2B. Mass spectrometry analysis revealed a novel acetylation site at an evolutionarily-conserved Lys 13 (K13) at the N-terminus of HOXB13 (Fig. 1A and Fig. S1A), that is absent in other HOX13 paralogs. Secondary protein structure prediction revealed that this lysine 13 is located within a 6-residue helical region (Fig. S1A)(30). To evaluate the functional relevance of this modification in PC, we developed and characterized a high-affinity monoclonal (2B7C1) and polyclonal antibodies (Abs) against acetylated lysine 13. Both antibodies specifically recognize only the acetylated K13-HOXB13 but not the unmodified HOXB13 (Fig. S1B). Subsequently, to identify the lysine acetyltransferase that promotes this specific modification, we co-expressed hemagglutinin (HA)-tagged HOXB13 in human embryonic kidney cells (HEK293T) together with known histone acetyltransferases (HATs) (Fig. S1C). Among these, two closely-related and evolutionary conserved HATs, cyclic adenosine monophosphate-responsive element-binding protein (CREB)-binding protein (CBP) and

Author Manuscript Author Manuscript Author Manuscript Author Manuscript

adenovirus E1A-associated 300-kDa protein (p300), acetylated the wild-type HOXB13 but not the HOXB13 mutated at K13 to the non-modifiable amino acids, alanine (K13A) or the arginine (K13R) (Figs. 1B and 1C). Additionally, the HOXB13-G84E PC risk variant was modified by p300 (Fig. 1B). Consistently, we detected an interaction of p300 with the wild-type but not with the recombinant HOXB13-K13A mutant (Fig. S1D). Significantly, we detected neither the acK13-HOXB13 nor the total HOXB13 protein in the normal prostate cell line, RWPE-1 (Fig. 1D). As opposed to RWPE-1, both AR-positive cell lines (VCaP, C4-2B, 22Rv1), and negative cell line (PC3) showed acK13-HOXB13, which is sensitive to a p300/CBP inhibitor (A-485) (Fig. 1D). Likewise, CBP-mediated nuclear localized wild-type HOXB13 shows loss of acetylation in response to A-485 treatment; by contrast, mutant *HOXB13K13A* is not acetylated (Fig. 1E). Consistently, C4-2B and VCaP showed a dose-dependent decrease in HOXB13-K13 acetylation following treatment with A-485 or GNE-049 (Figs. S1E–S1F). Moreover, A-485 sensitive HOXB13 acetylation is less susceptible to deprivation of glucose or acetate than CBP/p300 mediated histone H3K27 acetylation (Fig. S1G). To confirm CBP/p300 as the HAT, C4-2B, VCaP, and LAPC4. PC cell lines were transfected with either CBP alone or p300 silencing RNA alone or in combination. The ratio of acetylated to total HOXB13 is decreased when transfected with either CBP or p300 siRNA alone or in combination and is comparable to HOXB13 silencing (Fig. 1F–1I and Fig. S1H). A significant amount of acK13-HOXB13 expression is observed in human prostate cancers (Fig. S1I). These results reveal that HOXB13 is a bonafide CBP/p300 substrate.

Lysine 13 acetylated HOXB13 marks tumor promoting super-enhancers in hormone-naïve PCs

To examine the genome-wide distribution of acK13-HOXB13 in prostate cancer, we first validated the cognate antibodies for chromatin immunoprecipitation (ChIP) (Fig. S2A–S2F). Chromatin extracts prepared from C4-2B cells were transfected with either control or 2 independent CBP siRNAs followed by immunoprecipitation with acK13-HOXB13, pan-HOXB13 or IgG antibody. We detected acK13-HOXB13 binding at selective targets in the control siRNAs but not at *IGX1A* (control) in the CBP siRNA transfected cells (Fig. S2A–S2F). Consistently, the expression of these targets was decreased following CBP silencing (Fig. S2G). acK13-HOXB13 is also enriched at known CRPC targets in prostate tumors compared to normal validating the antibodies for ChIP (Figs. S2H–S2I).

To understand the relevance of this novel HOXB13-K13 acetylation in human prostate cancer, we characterized its binding, expression and function in well annotated clinical specimens (n=38; Table S1; Fig. S3A–S3B; Materials and Methods). As a first step, we performed ChIP-sequencing of matched human prostate normal and primary tumor tissues taken after radical prostatectomy (n=5: 2N and 3T; subset 1) with H3K27ac or acK13-HOXB13 antibodies (Fig. 2) or with pan-HOXB13, H3K27ac, acK13-HOXB13 or IgG antibodies (n=4; 2N and 2T; subset 2; Fig. S4). This analysis revealed an increased acK13-HOXB13 signal at the transcription start site (TSS) in tumor tissues compared to normal prostate and is consistent across multiple patient samples in both subsets (Fig. 2A and Fig. S4A). By contrast, the H3K27ac signal enrichment at peaks varied and were either higher or lower at TSSs in normal tissue compared to tumor depending on the subset (Fig.

Author Manuscript Author Manuscript Author Manuscript Author Manuscript

2B and Fig. S4A). A heatmap depicting acK13-HOXB13 and H3K27ac peaks within 1kb of the TSSs for the first subset is shown in Figs. 2C and 2D. Compared with the normal prostate, we observed a variation in the number of promoters with acK13-HOXB13 signals in tumors (27.6% tumor vs. 36.06% normal in subset 1 and 19% tumor vs. 16% normal in subset 2). However, there is consistent enrichment of acK13-HOXB13 signal within the transcribed portion of the gene in tumors, specifically at introns (24–39%) and at distal intergenic regions (22–39%) across both subsets. H3K27ac-enriched promoters in prostate tumors ranged from 14–18% in normal to 9–35% in tumors. In all cases, the distal intergenic regions had the highest proportion of pan-HOXB13 or acK13-HOXB13 signals at 39–45 % for acK13-HOXB13 or pan-HOXB13 antibody respectively. In order to determine whether tumor specific sites harbor increased acetylated HOXB13 signals compared to pan HOXB13 or H3K27ac we analyzed the ChIP sequencing data from subset 2. Our analysis revealed several thousand peaks for each antibody ChIP (Fig. S4A). A majority of the peaks were unique for each antibody. 4.6% of acK13-HOXB13 peaks in normal were retained in the tumor, while 16% of the acK13-HOXB13 peaks in tumors overlapped with the normal (Fig. S4B). In contrast, 1.76% of pan-HOXB13 peaks in normal were retained in the tumor, while 0.95% of the pan-HOXB13 in tumor overlapped with normal. Only 2.7% of the H3K27ac tumor peaks overlapped with the normal(Fig. S4B). These results suggest an increased occupancy of acetylated HOXB13 at the tumor specific sites even in the normal prostate.

As acK13-HOXB13 signals were higher than those expected at a typical enhancer, we determined whether the acK13-HOXB13 signal is differentially enriched at Super Enhancers (SEs) (27,31). We stratified SEs according to the strength of acK13-HOXB13 or pan-HOXB13 or H3K27ac signals (Figs. 2E to 2H; Figs. S4C–S4D). Even in the normal prostates, we detected increased acK13-HOXB13 signals at specific SEs (Fig. 2E) and were ~2 fold higher than pan-HOXB13 (Fig. S4D). In contrast, H3K27ac signals were same or 2-fold more intense at SEs in normal prostate than in tumor (Figs. 2F and 2H). In some cases, acK13-HOXB13 was further increased up to 3-fold at SE peaks in tumors, tracked with H3K27ac and higher than pan-HOXB13 (Fig. 2G and Fig. S4D). Subsequently, we analyzed ChIP-sequencing data to identify acK13-HOXB13-target genes regulated by SEs in tumors (Tables S2A and S2B). We identified 8% of genes overlapped in pan-HOXB13 versus acK13-HOXB13 in normal and tumor enriched SEs; this cohort included *HOXB13* as well as *ACK1/TNK2*, *SPON2*, *KLK3*, *BMPR1B* and *AURKB* (Figs. 2I–2K; Figs. S4E–S4H). ChIP-qPCR analysis confirmed acK13-HOXB13 enrichment at *ACK1* and *FOLH1* in primary prostate tumors compared to normal. Gene Set Enrichment Analysis (GSEA) revealed that in contrast to the normal prostate, which showed enrichment for both basal and luminal subtypes, the luminal epithelial subtype dominated in tumors. Importantly, we also observed a negative enrichment of tumor-specific SE-proximal genes in normal prostate (normal: NES = −1.563, $p = 0.007$ *vs.* tumor: NES = 2.695, $p = 0.000$) (Figs. 2L–2M). Our analysis of TF motifs at acK13-HOXB13 binding sites revealed enrichment of SMAD2 and MAFA binding motifs (Fig. 2N). In contrast, the most common TF motifs at acK13-HOXB13 binding sites were those of factors associated with epithelial-mesenchymal transition (Fig. 2O).

Subsequently, we analyzed the expression of acK13-HOXB13 regulated super-enhancer targets (*HOXB13, AR, ACK1, FOLH1 (PSMA), VEGFA,* and *SPON2*) in matched human

Author Manuscript Author Manuscript Author Manuscript Author Manuscript

normal and prostate tumors (n=38; total: 19N and 19T); acetylated HOXB13 signals were significantly upregulated in tumors compared to normal (Fig. 3A). In order to investigate the role of acK13-HOXB13 regulated SE linked genes in PC pathogenesis, we focused on a representative CRPC target, ACK1 tyrosine kinase, which had acquired a tumor specific SE (SE rank 677 and 548 in RP #1 and rank 146 in RP #2) (Fig. 3B; Fig. S4E), correlating with increased recruitment of acetylated HOXB13 (Fig S4E) and expression of ACK1 mRNA and protein (Figs. 3A and 3C). We detected increased phosphorylated ACK1 (pY284-ACK) associated with kinase activation HOXB13 and AR expression in tumors compared to normal and benign prostatic hyperplasia (BPH) (Fig. 3D).

Super Enhancers are retained in metastatic CRPC despite androgen deprivation

To corroborate the role of HOXB13-K13 acetylation in prostate cancer, we first examined its role in C4-2B followed by validation in additional PC lines (VCaP and 22Rv1). ChIP followed by deep sequencing of androgen-deprived C4-2B revealed a significant enrichment of acK13-HOXB13 at ~46,684 sites comprising distal intergenic regions and promoters across the genome (Fig. 4A). Approximately 85% of the acK13-HOXB13-K13 binding sites were located within ~2 kb of (TSS) and another 10% were identified at distal enhancers (Fig. 4B). The acK13-HOXB13 binding motif is enriched for the GTAAACA sequence that differs from unmodified HOXB13 motifs CCAATAAA and CTCGTAAA (32) (Fig. 4C). Other most frequently detected DNA motifs enriched include Zinc finger protein and X-linked factor (ZFX), and AR element (ARE)-half sites (Fig. 4C and Table S3).

We uncovered broad HOXB13-K13 acetylation peaks in the vicinity of *HOXB13*, as well as several lineage and prostate tissue-specific genes *NKX3-1*, *PMEPA1*, *SLC45A3*, *PSCA*, *KLK*s, oncogenes *MYC*, *BCL6,* mitotic kinase *AURKB*, *AR* and *ACK1/TNK2* and novel targets *FOLH1, RXRA*, *NFIX* and *ZBTB16* (Fig. 4D, Figs. S5A). At proximal TSSs, acK13-HOXB13 enrichment signals overlapped with H3K27ac, H3K4me2/3, and RNA Pol II binding peaks (Fig. S5A). At distal TSS sites, the acK13-HOXB13 peaks overlapped with H3K27ac and H3K4me2 marks suggesting that acK13-HOXB13 marked regions may represent spatially-distinct enhancers (Fig. 4D and Fig. S5A; Table S4). Furthermore, Hi-C chromatin conformation capture prediction analysis revealed H3K27ac and acK13-HOXB13 chromatin loop interactions at the *ACK1* genomic locus (Fig. S5B)(33). Approximately 50% of acK13-HOXB13 binding sites overlap with those of genome-wide H3K27ac peaks and occupied long tracks of several kilobases in length (Fig. S5C). Consistently, we confirmed that acetylated HOXB13 interacts with the chromatin looping factor CTCF (Fig. S5D). ROSE analysis revealed 619, 592, and 632 acK13-HOXB13 or H3K27ac peak-enriched SEs (Figs. 4E to 4G). Furthermore, 388 out of the 592 (65.5%) H3K27ac signal enriched SEs overlapped with acK13-HOXB13, while 204 SEs were unique (Table S5). We validated acK13-HOXB13 at *BMPR1B* and *AR* by directed ChIP-qPCR (Figs. S5E and S5F). In contrast, we found that *AURKB,* is targeted by both HOXB13 and acK13-HOXB13 (17).

To determine whether acK13-HOXB13 at TSS and SEs might be due to increased HOXB13 expression in PCs, we performed ROSE analysis which revealed 632 SEs with acK13-HOXB13 after normalizing for input compared to 675 SEs after normalizing for pan-HOXB13 with a majority enriched for acK13-HOXB13 (Fig. S6A; Table S6A). A

Author Manuscript Author Manuscript Author Manuscript Author Manuscript

representative enrichment at *ACK1/TNK2* and *FOLH1* is shown (Fig. S6B). We conducted ChIP-sequencing using isogenic parental (C4-2B and 22Rv1) and their corresponding *HOXB13K13A* mutants so as to determine how much the acK13-antibody is picking up peaks as well as SEs in the *HOXB13K13A* mutant expressing cells. Bioinformatics analysis revealed acK13-HOXB13 unique peaks in both C4-2B and 22Rv1 cell lines at ~70%, while there were fewer than 5% unique peaks in the corresponding *HOXB13K13A* mutant expressing cells (Fig. S6C–S6D). ROSE analysis revealed unique acK13-HOXB13 specific signal enriched SEs in parental at ~76% versus *HOXB13K13A* mutant at ~1.4% (Fig. S6E–S6F, Table S6B). Treatment of PC lines with the CBP/p300 inhibitor reduced mRNA expression of representative acK13-HOXB13 SE regulated targets (Fig. S6G–S6H). Overall, these results indicate that a majority of the SEs were specifically enriched for acK13-HOXB13 signals.

HOXB13-acetylation target gene expression is enriched in CRPCs

To investigate whether the high intensity acK13-HOXB13 signal-enriched SE target genes are associated with pathogenesis, we performed Gene-Set Enrichment Analysis (GSEA) analysis. GSEA revealed a significant enrichment for acK13-HOXB13 SE-proximal targets in mCRPCs (n=260) compared to primary PC (n=1061) (normalized enrichment score [NES] = 1.392, false discovery rate [FDR] $q = 0.022$) and in primary PCs (n=1061) compared to normal (n=794) (NES = 1.955; FDR $q = 0.000$) (Fig. 4H) (34). To examine the functional impact of the enriched CRPC-SEs, we integrated the acK13-HOXB13 peak enriched SE proximal genes with the genes that were differentially expressed (DEGs) following *HOXB13* ablation (17,23). A significant enrichment of SE-regulated genes of the primary luminal epithelial subtype was observed in primary PCs (NES = 1.998; FDR $q = 0.000$) (Fig. 4I). Of the 2,540 HOXB13-associated DEGs, 1307 (51.4 %) harbored an acK13-HOXB13 enhancer within 500 kb of the TSS; 194 (7.6%) had an H3K27ac signal-enriched SE and 186 (7.3%) had an acK13-HOXB13 signal-enriched SE (Table S7).

To validate the activation of acK13-HOXB13-enriched SE-proximal genes in a larger cancer dataset, we performed t-distributed stochastic neighbor embedding (t-SNE) analysis of these genes in The Cancer Genome Atlas Prostate Adenocarcinoma (TCGA-PRAD) dataset. A heatmap examining this expression revealed no specific pattern in the normal prostate dataset, but uncovered two prominent clusters in tumors (Figs. S7A and S7B). These clusters are enriched for genes associated with angiogenesis *ANG, VANGL1,* and *ANGPTL 3–4*, enzyme regulators such as *ACK1/TNK2* and *PPP1R9B*. (Fig. S7C). Directed ChIP-qPCR validated acK13-HOXB13 binding at these targets, which also was not impacted following treatment with Enzalutamide (Figs. S7D and S7E). Subsequently, we confirmed increased expression of ANGPTL3 and ANGPTL4 in primary tumors by quantitative gene expression analysis (Fig. S7F).

ACK1 and *FOLH1* are actionable targets of HOXB13 upregulated PCs

To further validate the actionable targets of acK13-HOXB13 epigenome, we examined two critical targets, *ACK1* and *FOLH1.* ACK1 autophosphorylation at Tyr284 leading to its kinase activation is increased in CRPCs, enriched in stem-like cells and is linked to poor prognosis (7,35,36). A potent ACK1 small molecule inhibitor (R)-9b is also reported

Author Manuscript Author Manuscript Author Manuscript Author Manuscript

(Fig. 4J) (28). The acK13-HOXB13 and H3K27 acetylation-signal enriched SE of *ACK1* starts upstream of TSS and extends into Intron I (Fig. 4J). Directed ChIP-qPCR validated acK13-HOXB13 binding at the SEs of the *ACK1* genomic locus in C4-2B, but not at the control *IGX1A* locus (Fig. 4K).

FOLH1, encodes the prostate-specific membrane antigen (PSMA) (Fig. S8A). The radioligand of PSMA, ^{68}Ga-PSMA 11-PET (RLT), and the recently approved ^{177}Lu-PSMA-617 are US Food and Drug Administration (FDA)-approved diagnostic or therapeutic for metastatic CRPCs (37–39). We validated the binding of acK13-HOXB13 to a genomic region proximal to *FOLH1* by directed ChIP-qPCR (Fig. S8B and Fig. S2F). Furthermore, siRNA-mediated depletion of HOXB13 led to a decrease in *FOLH1* expression in C4-2B, VCaP, and 22Rv1 cells (Figs. S8C–S8E). Moreover, the level of *FOLH1* mRNA expression correlated with HOXB13 mRNA levels in both primary and metastatic PCs (Figs. S8F to S8G). These results collectively confirm *ACK1* and *FOLH1* as direct transcriptional targets of acK13-HOXB13.

Acetylated HOXB13-K13 differentially interacts with SWI/SNF chromatin remodeling proteins

To investigate the molecular mechanism by which acK13-HOXB13 drives CRPC SE selection, we performed affinity pulldown with biotinylated unmodified and lysine13 modified HOXB13 peptides (1–25 amino acids) followed by mass spectrometry (Fig. S9A). Proteomic analysis revealed a differential enrichment of proteins binding the acK13 peptide compared to the unmodified control HOXB13 peptide (Fig. S9B). Proteins enriched in the acK13-HOXB13 peptide pulldown included the SWI/SNF chromatin remodeling proteins SNF2L1/SMARCC1, the bromodomain containing proteins (BAZ2B, SMARCA2, BRD7 and BRD9)(40), DAXX, as well the chromatin looping protein CTCF (Fig. S9C; Table S8). In contrast, both modified and unmodified HOXB13 N-terminal peptides equally bound members of the transcription pre-initiation complex, including TAF1A/B/C/D and TAF3 associated with RNA Polymerase II (41,42) (Fig. S9C–S9D). To confirm BRD9 as a direct reader of K13 acetylation, we tested binding with modified and unmodified biotinylated HOXB13-K13 peptides. BRD9 binds specifically to acetylated HOXB13 but not the unmodified peptide and persists in the presence of H4K5ac peptide (Fig. S9E). Co-immunoprecipitation studies revealed interaction of acetylated HOXB13 with BRD9 in C4-2B and VCaP, and this interaction is abolished in the *HOXB13K13A* mutant (Fig. S9F–S9G).

HOXB13K13A mutants show impaired colony formation and xenograft tumor growth

As acetylated K13-HOXB13 is enriched at super enhancers proximal to CRPC associated target genes, we examined the impact of effect of *HOXB13K13A* mutation in C4-2B and 22Rv1 cell lines. *HOXB13K13A* point mutants had undetectable levels of K13-acetylation in both cell lines and with a significant decrease in the expression of HOXB13, ACK1 and PSMA proteins (Fig. 5A and Fig. S10A). Functionally, *HOXB13K13A* exhibited reduced cell proliferation, comparable to the C4-2B *HOXB13-pKO* deletion mutant (17) (Fig. 5B; Fig. S10B). *HOXB13K13A* point mutants display decrease in number and size of the colonies (Fig. 5C; Fig. S10C), reduced 3-dimensional (3D) spheroid formation that indicated

Author Manuscript Author Manuscript Author Manuscript Author Manuscript

a failure to self-renew and self-organize (Fig. 5D; Fig. S10C–S10E). Next, to examine resistance to AR-targeted therapies, we treated isogenic parental and *HOXB13K13A* mutants with enzalutamide (ENZ). Treatment with the ENZ caused a rounding up and decreased colony formation of the *HOXB13K13A* mutant (Fig. 5E; Fig. S10F–S10G). While the C4-2B parental cells are highly resistant to ENZ (IC_{50} = 64 μM), the isogenic *HOXB13K13A* (IC_{50}= 10–19 μM) and the *HOXB13pKO* deletion mutants (IC_{50} = 12.15 μM) had lowered resistance, with a 3–5-fold increase in the sensitivity to ENZ (Fig. 5F). The levels of acK13-HOXB13 increased in response to ENZ and decreased in response to the Bromodomain and Extra-Terminal (BET) bromodomain inhibitor, JQ1 (Fig. 5G). Moreover, C4-2B *HOXB13K13A* mutant displayed reduced H3K27 acetylation but not the H4K12 acetylation (Fig. 5H). Notably, the *HOXB13K13A* mutants (Figs. 5I to 5K, Figs. S11A to S11C) formed significantly smaller xenograft tumors in male SCID mice with downregulation of ACK1 and PSMA/FOLH1 proteins (Fig. S11D) and angiopoietin gene expression (*ANG, ANGPT2, ANGPTL3,* and *ANGPTL4*) compared to isogenic parental control (Figs. S11E–S11F). Additionally, flow cytometry analysis confirmed downregulation of PSMA in the *HOXB13K13A* mutant compared to the parental cells (Fig. 5L). Differential gene expression (DEGs) analysis revealed 103 of 113 genes harbored at least one acK13-HOXB13 peak within 500 kb of their TSS (Table S9). Furthermore, Gene Ontology (GO) analysis revealed enrichment of chromatin remodeling and self-renewal genes as top targets.

HOXB13K13A spheroid growth and anti-androgen resistance can be rescued by restoring acetylation.

To determine how the loss of acK13-HOXB13 impacts CRPC xenograft tumor growth, we analyzed its recruitment to CRPC-associated targets (Fig. 6A). Directed ChIP-qPCR analysis revealed acK13-HOXB13 binding persisted at the SEs following treatment with the anti-androgen Enzalutamide (Figs. 6B–6D). Consistently, acetylated HOXB13 recruitment is reduced in the *HOXB13K13A* mutant but not in the parental cells at the representative SE targets (Fig. S12A). Subsequently, we tested whether restoring HOXB13-WT rescues some of the phenotypes observed in the acetylation-defective K13A mutant (Fig. S12B). Individual clones from GFP-tagged vector, HOXB13-WT or the *HOXB13K13A* mutant were flow-sorted, confirmed by western blotting (Fig. S12C) and analyzed for spheroid formation and enzalutamide sensitivity (Fig. S12D–S12E). We recovered significantly larger spheroids in the wild-type HOXB13 compared to the *HOXB13K13A* mutant expressing cells (Fig. S12D) that were also resistant to Enzalutamide (Fig. S12E). Consistently, *HOXB13K13A* mutants show reduced expression of SE associated targets (Fig. S12F).

ACK1 inhibitor (R)-9b sensitizes drug-resistant human prostate tumor organoids

As TFs are not directly druggable, we pursued targets amenable to therapeutic intervention. To investigate HOXB13-ACK1 axis in prostate tumor development, we performed single-cell RNA-sequencing of human prostate organoids (43,44). HOXB13, AR and ACK1 expression was seen in 11 sub clusters in the normal prostate organoids by t-distributed stochastic neighbor embedding (t-SNE) analysis (Figs. S6E–S6G). Further delineation of the sub clusters based on the expression of NKX3-1 (luminal epithelial stem cell marker), ZEB 1 (basal epithelial stem cell marker) revealed the presence of progenitor cells expressing both NKX3.1 and ZEB1(Fig. 6H and Fig. S13) (13,45). As ACK1/TNK2 is expressed within

Author Manuscript Author Manuscript Author Manuscript Author Manuscript

the multiple sub clusters (Fig. 6F), we compared the sensitivity of the normal and tumor derived prostate organoids to the selective ACK1 inhibitor (R)-9b and the AR antagonists ENZ or abiraterone (Figs. 6I–6K). Human prostate tumor organoids display significant sensitivity to (R)-9b, fairly resistant to Enzalutamide and modestly sensitive to Abiraterone (Fig. 6K). Collectively, our studies underscore for the first time ACK1 tyrosine kinase as an actionable target of HOXB13 deregulated prostate cancers.

Discussion

This study reveals that acetylation of HOXB13 at lysine 13 transforms it into a pro-CRPC transcription factor. While pioneer TFs, including HOXB13, can access their target sites within compacted chromatin, and thus are capable of initiating the earliest steps of transcription, whether their chromatin binding activity is regulated is not known (32). p300 and CBP are two closely-related lysine acetyltransferases that function as transcriptional coactivators by engaging lineage-specific TFs at specific enhancers to control cell and tissue identity (24,25). Our studies elucidate for the first time a close co-operation between HOXB13 and p300/CBP to promote epigenetic marking at enhancers and super-enhancers in cancer cells. These results also suggest that while normal levels of gene expression are maintained by histone H3K27 acetylation, the high levels of gene expression observed in tumors is dependent on the activity of K13 acetylated HOXB13.

Chromatin binding studies indicate that binding of acK13-HOXB13 overlaps with sites of H3K27 acetylation at several characterized SEs, notably those controlling the expression of the AR pathway genes (*AR* and *KLK3*), tissue-identity genes (*SLC45A3*/Prostein, *SPON2*, *PSCA*, and *FOLH1*) and angiopoietins (*ANG1, ANGPTL3,* and *ANGPTL4*). As a group, these genes confer prostate-tissue type characteristics at SEs and some occur *de novo* such as the oncogene *ACK1* tyrosine kinase, which is a critical regulator of CRPC growth. In CRPCs, ACK1 expression is high, which in turn promotes the expression of the *AR* and androgen-independent AR-mediated transcriptional activity (7,28). Consistently, activation of ACK1 and downstream signaling protects the cells from lethal irradiation, replicative stress and DNA damage (46,47). ACK1 is also a target of the E3 ubiquitin ligases SIAH1 and SIAH2 in hormone-associated breast cancers (48). However, prior to this study, it was not clear how ACK1 is upregulated in PCs. Our studies revealed that acetylated HOXB13 has a direct role in *ACK1* gene regulation in PC via its capacity to establish a CRPC-specific SE. Increased ACK1 expression overrides the loss of androgen stimulation consistent with the sensitivity to (R)-9b (28). In summary, our data demonstrate that acetylated HOXB13 mediated CRPC-SEs are critical mediators of anti-androgen resistance.

Supplementary Material

Refer to Web version on PubMed Central for supplementary material.

Acknowledgements

K.M. acknowledges support from the Phi Beta Psi Sorority, Department of Defense W81XWH-21-1-0203, by an NCATS Clinical and Translational Sciences Award, #UL1 TR002345 and the Department of Surgery at Washington University. N.P. Mahajan is a recipient of NIH/NCI grants (1R01CA208258 and 5R01CA227025), Prostate Cancer Foundation (PCF) grant (17CHAL06) and Department of Defense grant (W81XWH-21-1-0202). The WU-PSR

Author Manuscript Author Manuscript Author Manuscript Author Manuscript

is supported in part by the WU Institute of Clinical and Translational Sciences (NCATS UL1 TR000448), the Mass Spectrometry Research Resource (NIGMS P41 GM103422; R24GM136766) and the Siteman Comprehensive Cancer Center Support Grant (NCI P30 CA091842). The Siteman Cancer Center is supported in part by an NCI Cancer Center Support Grant #P30 CA091842.

References

1. Bray F, Ferlay J, Soerjomataram I, Siegel RL, Torre LA, Jemal A. Global cancer statistics 2018: GLOBOCAN estimates of incidence and mortality worldwide for 36 cancers in 185 countries. CA: a cancer journal for clinicians 2018;68(6):394–424 doi 10.3322/caac.21492. [PubMed: 30207593]
2. Robinson D, Van Allen EM, Wu YM, Schultz N, Lonigro RJ, Mosquera JM, et al. Integrative clinical genomics of advanced prostate cancer. Cell 2015;161(5):1215–28 doi 10.1016/j.cell.2015.05.001. [PubMed: 26000489]
3. Wyatt AW, Gleave ME. Targeting the adaptive molecular landscape of castration-resistant prostate cancer. EMBO Mol Med 2015;7(7):878–94 doi 10.15252/emmm.201303701. [PubMed: 25896606]
4. Kim EH, Andriole GL. Prostate Cancer Review. Mo Med 2018;115(2):131. [PubMed: 30228703]
5. Takeda DY, Spisak S, Seo JH, Bell C, O'Connor E, Korthauer K, et al. A Somatically Acquired Enhancer of the Androgen Receptor Is a Noncoding Driver in Advanced Prostate Cancer. Cell 2018;174(2):422–32 e13 doi 10.1016/j.cell.2018.05.037. [PubMed: 29909987]
6. Shah N, Wang P, Wongvipat J, Karthaus WR, Abida W, Armenia J, et al. Regulation of the glucocorticoid receptor via a BET-dependent enhancer drives antiandrogen resistance in prostate cancer. Elife 2017;6 doi 10.7554/eLife.27861.
7. Mahajan NP, Coppola D, Kim J, Lawrence HR, Lawrence NJ, Mahajan K. Blockade of ACK1/TNK2 To Squelch the Survival of Prostate Cancer Stem-like Cells. Sci Rep 2018;8(1):1954 doi 10.1038/s41598-018-20172-z. [PubMed: 29386546]
8. Zhang L, Jiao M, Li L, Wu D, Wu K, Li X, et al. Tumorspheres derived from prostate cancer cells possess chemoresistant and cancer stem cell properties. J Cancer Res Clin Oncol 2012;138(4):675–86 doi 10.1007/s00432-011-1146-2. [PubMed: 22237455]
9. Chen X, Li Q, Liu X, Liu C, Liu R, Rycaj K, et al. Defining a Population of Stem-like Human Prostate Cancer Cells That Can Generate and Propagate Castration-Resistant Prostate Cancer. Clin Cancer Res 2016;22(17):4505–16 doi 10.1158/1078-0432.CCR-15-2956. [PubMed: 27060154]
10. Mani SA, Guo W, Liao MJ, Eaton EN, Ayyanan A, Zhou AY, et al. The epithelial-mesenchymal transition generates cells with properties of stem cells. Cell 2008;133(4):704–15 doi 10.1016/j.cell.2008.03.027. [PubMed: 18485877]
11. Soundararajan R, Paranjape AN, Barsan V, Chang JT, Mani SA. A novel embryonic plasticity gene signature that predicts metastatic competence and clinical outcome. Sci Rep 2015;5:11766 doi 10.1038/srep11766. [PubMed: 26123483]
12. Pomerantz MM, Qiu X, Zhu Y, Takeda DY, Pan W, Baca SC, et al. Prostate cancer reactivates developmental epigenomic programs during metastatic progression. Nat Genet 2020;52(8):790–9 doi 10.1038/s41588-020-0664-8. [PubMed: 32690948]
13. Le Magnen C, Shen MM, Abate-Shen C. Lineage Plasticity in Cancer Progression and Treatment. Annu Rev Cancer Biol 2018;2:271–89 doi 10.1146/annurev-cancerbio-030617-050224. [PubMed: 29756093]
14. Urbanucci A, Barfeld SJ, Kytola V, Itkonen HM, Coleman IM, Vodak D, et al. Androgen Receptor Deregulation Drives Bromodomain-Mediated Chromatin Alterations in Prostate Cancer. Cell Rep 2017;19(10):2045–59 doi 10.1016/j.celrep.2017.05.049. [PubMed: 28591577]
15. Corces MR, Buenrostro JD, Wu B, Greenside PG, Chan SM, Koenig JL, et al. Lineage-specific and single-cell chromatin accessibility charts human hematopoiesis and leukemia evolution. Nat Genet 2016;48(10):1193–203 doi 10.1038/ng.3646. [PubMed: 27526324]
16. Norris JD, Chang CY, Wittmann BM, Kunder RS, Cui H, Fan D, et al. The homeodomain protein HOXB13 regulates the cellular response to androgens. Mol Cell 2009;36(3):405–16 doi 10.1016/j.molcel.2009.10.020. [PubMed: 19917249]
17. Nerlakanti N, Yao J, Nguyen DT, Patel AK, Eroshkin AM, Lawrence HR, et al. Targeting the BRD4-HOXB13 Coregulated Transcriptional Networks with Bromodomain-Kinase Inhibitors to

Author Manuscript Author Manuscript Author Manuscript Author Manuscript

Suppress Metastatic Castration-Resistant Prostate Cancer. Mol Cancer Ther 2018;17(12):2796–810 doi 10.1158/1535-7163.MCT-18-0602. [PubMed: 30242092]

18. Kim EH, Cao D, Mahajan NP, Andriole GL, Mahajan K. ACK1-AR and AR-HOXB13 signaling axes: epigenetic regulation of lethal prostate cancers. NAR Cancer 2020;2(3):zcaa018 doi 10.1093/narcan/zcaa018. [PubMed: 32885168]
19. Ewing CM, Ray AM, Lange EM, Zuhlke KA, Robbins CM, Tembe WD, et al. Germline mutations in HOXB13 and prostate-cancer risk. N Engl J Med 2012;366(2):141–9 doi 10.1056/NEJMoa1110000. [PubMed: 22236224]
20. Beebe-Dimmer JL, Hathcock M, Yee C, Okoth LA, Ewing CM, Isaacs WB, et al. The HOXB13 G84E Mutation Is Associated with an Increased Risk for Prostate Cancer and Other Malignancies. Cancer Epidemiol Biomarkers Prev 2015;24(9):1366–72 doi 10.1158/1055-9965.EPI-15-0247. [PubMed: 26108461]
21. Zabalza CV, Adam M, Burdelski C, Wilczak W, Wittmer C, Kraft S, et al. HOXB13 overexpression is an independent predictor of early PSA recurrence in prostate cancer treated by radical prostatectomy. Oncotarget 2015;6(14):12822–34 doi 10.18632/oncotarget.3431. [PubMed: 25825985]
22. Weiner AB, Faisal FA, Davicioni E, Karnes RJ, Griend DJV, Lotan TL, et al. Somatic HOXB13 Expression Correlates with Metastatic Progression in Men with Localized Prostate Cancer Following Radical Prostatectomy. Eur Urol Oncol 2020 doi 10.1016/j.euo.2020.05.001.
23. Yao J, Chen Y, Nguyen DT, Thompson ZJ, Eroshkin AM, Nerlakanti N, et al. The Homeobox gene, HOXB13, Regulates a Mitotic Protein-Kinase Interaction Network in Metastatic Prostate Cancers. Sci Rep 2019;9(1):9715 doi 10.1038/s41598-019-46064-4. [PubMed: 31273254]
24. Lasko LM, Jakob CG, Edalji RP, Qiu W, Montgomery D, Digiammarino EL, et al. Discovery of a selective catalytic p300/CBP inhibitor that targets lineage-specific tumours. Nature 2017;550(7674):128–32 doi 10.1038/nature24028. [PubMed: 28953875]
25. Weinert BT, Narita T, Satpathy S, Srinivasan B, Hansen BK, Scholz C, et al. Time-Resolved Analysis Reveals Rapid Dynamics and Broad Scope of the CBP/p300 Acetylome. Cell 2018;174(1):231–44 e12 doi 10.1016/j.cell.2018.04.033. [PubMed: 29804834]
26. Loven J, Hoke HA, Lin CY, Lau A, Orlando DA, Vakoc CR, et al. Selective inhibition of tumor oncogenes by disruption of super-enhancers. Cell 2013;153(2):320–34 doi 10.1016/j.cell.2013.03.036. [PubMed: 23582323]
27. Whyte WA, Orlando DA, Hnisz D, Abraham BJ, Lin CY, Kagey MH, et al. Master transcription factors and mediator establish super-enhancers at key cell identity genes. Cell 2013;153(2):307–19 doi 10.1016/j.cell.2013.03.035. [PubMed: 23582322]
28. Mahajan K, Malla P, Lawrence HR, Chen Z, Kumar-Sinha C, Malik R, et al. ACK1/TNK2 Regulates Histone H4 Tyr88-phosphorylation and AR Gene Expression in Castration-Resistant Prostate Cancer. Cancer Cell 2017;31(6):790–803 e8 doi 10.1016/j.ccell.2017.05.003. [PubMed: 28609657]
29. Drost J, Karthaus WR, Gao D, Driehuis E, Sawyers CL, Chen Y, et al. Organoid culture systems for prostate epithelial and cancer tissue. Nat Protoc 2016;11(2):347–58 doi 10.1038/nprot.2016.006. [PubMed: 26797458]
30. Xu D, Zhang Y. Toward optimal fragment generations for ab initio protein structure assembly. Proteins 2013;81(2):229–39 doi 10.1002/prot.24179. [PubMed: 22972754]
31. Hnisz D, Abraham BJ, Lee TI, Lau A, Saint-Andre V, Sigova AA, et al. Super-enhancers in the control of cell identity and disease. Cell 2013;155(4):934–47 doi 10.1016/j.cell.2013.09.053. [PubMed: 24119843]
32. Morgunova E, Yin Y, Das PK, Jolma A, Zhu F, Popov A, et al. Two distinct DNA sequences recognized by transcription factors represent enthalpy and entropy optima. Elife 2018;7 doi 10.7554/eLife.32963.
33. Yardimci GG, Noble WS. Software tools for visualizing Hi-C data. Genome Biol 2017;18(1):26 doi 10.1186/s13059-017-1161-y. [PubMed: 28159004]
34. You S, Knudsen BS, Erho N, Alshalalfa M, Takhar M, Al-Deen Ashab H, et al. Integrated Classification of Prostate Cancer Reveals a Novel Luminal Subtype with Poor Outcome. Cancer Res 2016;76(17):4948–58 doi 10.1158/0008-5472.CAN-16-0902. [PubMed: 27302169]

Author Manuscript Author Manuscript Author Manuscript Author Manuscript

35. Mahajan K, Coppola D, Rawal B, Chen YA, Lawrence HR, Engelman RW, et al. Ack1-mediated androgen receptor phosphorylation modulates radiation resistance in castration-resistant prostate cancer. J Biol Chem 2012;287(26):22112–22 doi 10.1074/jbc.M112.357384. [PubMed: 22566699]
36. Mahajan K, Challa S, Coppola D, Lawrence H, Luo Y, Gevariya H, et al. Effect of Ack1 tyrosine kinase inhibitor on ligand-independent androgen receptor activity. Prostate 2010;70(12):1274–85 doi 10.1002/pros.21163. [PubMed: 20623637]
37. Moghul M, Somani B, Lane T, Vasdev N, Chaplin B, Peedell C, et al. Detection rates of recurrent prostate cancer: (68)Gallium (Ga)-labelled prostate-specific membrane antigen versus choline PET/CT scans. A systematic review. Ther Adv Urol 2019;11:1756287218815793 doi 10.1177/1756287218815793. [PubMed: 30671137]
38. Kimura S, Abufaraj M, Janisch F, Iwata T, Parizi MK, Foerster B, et al. Performance of [(68)Ga] Ga-PSMA 11 PET for detecting prostate cancer in the lymph nodes before salvage lymph node dissection: a systematic review and meta-analysis. Prostate Cancer Prostatic Dis 2019 doi 10.1038/s41391-019-0156-z.
39. Sartor O, de Bono J, Chi KN, Fizazi K, Herrmann K, Rahbar K, et al. Lutetium-177-PSMA-617 for Metastatic Castration-Resistant Prostate Cancer. N Engl J Med 2021;385(12):1091–103 doi 10.1056/NEJMoa2107322. [PubMed: 34161051]
40. Mashtalir N, D'Avino AR, Michel BC, Luo J, Pan J, Otto JE, et al. Modular Organization and Assembly of SWI/SNF Family Chromatin Remodeling Complexes. Cell 2018;175(5):1272–88 e20 doi 10.1016/j.cell.2018.09.032. [PubMed: 30343899]
41. Baptista T, Grunberg S, Minoungou N, Koster MJE, Timmers HTM, Hahn S, et al. SAGA Is a General Cofactor for RNA Polymerase II Transcription. Mol Cell 2017;68(1):130–43 e5 doi 10.1016/j.molcel.2017.08.016. [PubMed: 28918903]
42. Warfield L, Ramachandran S, Baptista T, Devys D, Tora L, Hahn S. Transcription of Nearly All Yeast RNA Polymerase II-Transcribed Genes Is Dependent on Transcription Factor TFIID. Mol Cell 2017;68(1):118–29 e5 doi 10.1016/j.molcel.2017.08.014. [PubMed: 28918900]
43. McCray T, Moline D, Baumann B, Vander Griend DJ, Nonn L. Single-cell RNA-Seq analysis identifies a putative epithelial stem cell population in human primary prostate cells in monolayer and organoid culture conditions. Am J Clin Exp Urol 2019;7(3):123–38. [PubMed: 31317052]
44. Puca L, Bareja R, Prandi D, Shaw R, Benelli M, Karthaus WR, et al. Patient derived organoids to model rare prostate cancer phenotypes. Nat Commun 2018;9(1):2404 doi 10.1038/s41467-018-04495-z. [PubMed: 29921838]
45. Wang X, Xu H, Cheng C, Ji Z, Zhao H, Sheng Y, et al. Identification of a Zeb1 expressing basal stem cell subpopulation in the prostate. Nat Commun 2020;11(1):706 doi 10.1038/s41467-020-14296-y. [PubMed: 32024836]
46. Mahendrarajah N, Borisova ME, Reichardt S, Godmann M, Sellmer A, Mahboobi S, et al. HSP90 is necessary for the ACK1-dependent phosphorylation of STAT1 and STAT3. Cell Signal 2017;39:9–17 doi 10.1016/j.cellsig.2017.07.014. [PubMed: 28739485]
47. Mahendrarajah N, Paulus R, Kramer OH. Histone deacetylase inhibitors induce proteolysis of activated CDC42-associated kinase-1 in leukemic cells. J Cancer Res Clin Oncol 2016;142(11):2263–73 doi 10.1007/s00432-016-2229-x. [PubMed: 27576506]
48. Knauer SK, Mahendrarajah N, Roos WP, Kramer OH. The inducible E3 ubiquitin ligases SIAH1 and SIAH2 perform critical roles in breast and prostate cancers. Cytokine Growth Factor Rev 2015;26(4):405–13 doi 10.1016/j.cytogfr.2015.04.002. [PubMed: 26028498]

Author Manuscript Author Manuscript Author Manuscript Author Manuscript

Statement of Translational Relevance

HOXB13, a prostate-enriched transcription factor, is associated with lethal CRPC progression. However, to date targeting it clinically to improve patient outcomes has not been feasible. We have uncovered that CBP/p300 histone acetyl transferase specifically targets HOXB13 for acetylation in prostate cancer cells. This K13-acetylated HOXB13 is enriched at tumor-specific super enhancers, and regulates its own gene expression, as well as the CRPC target genes, *ACK1* and *FOLH1* (PSMA). Acetylation-defective HOXB13 CRPC mutant shows reduced ACK1 and PSMA levels, is sensitive to anti-androgens and significantly impaired in xenograft tumor growth, underscoring the clinical relevance of targeting this HOXB13-ACK1 axis to block CRPC progression. Consistently, HOXB13 expressing human prostate tumors organoids but not normal are resistant to anti-androgens and sensitive to the first-in-class ACK1 inhibitor (R)-9b. Collectively, these studies highlight a role for the newly identified acetylated HOXB13 as a clinically relevant biomarker and an epigenetic regulator of CRPC progression.

Author Manuscript Author Manuscript Author Manuscript Author Manuscript

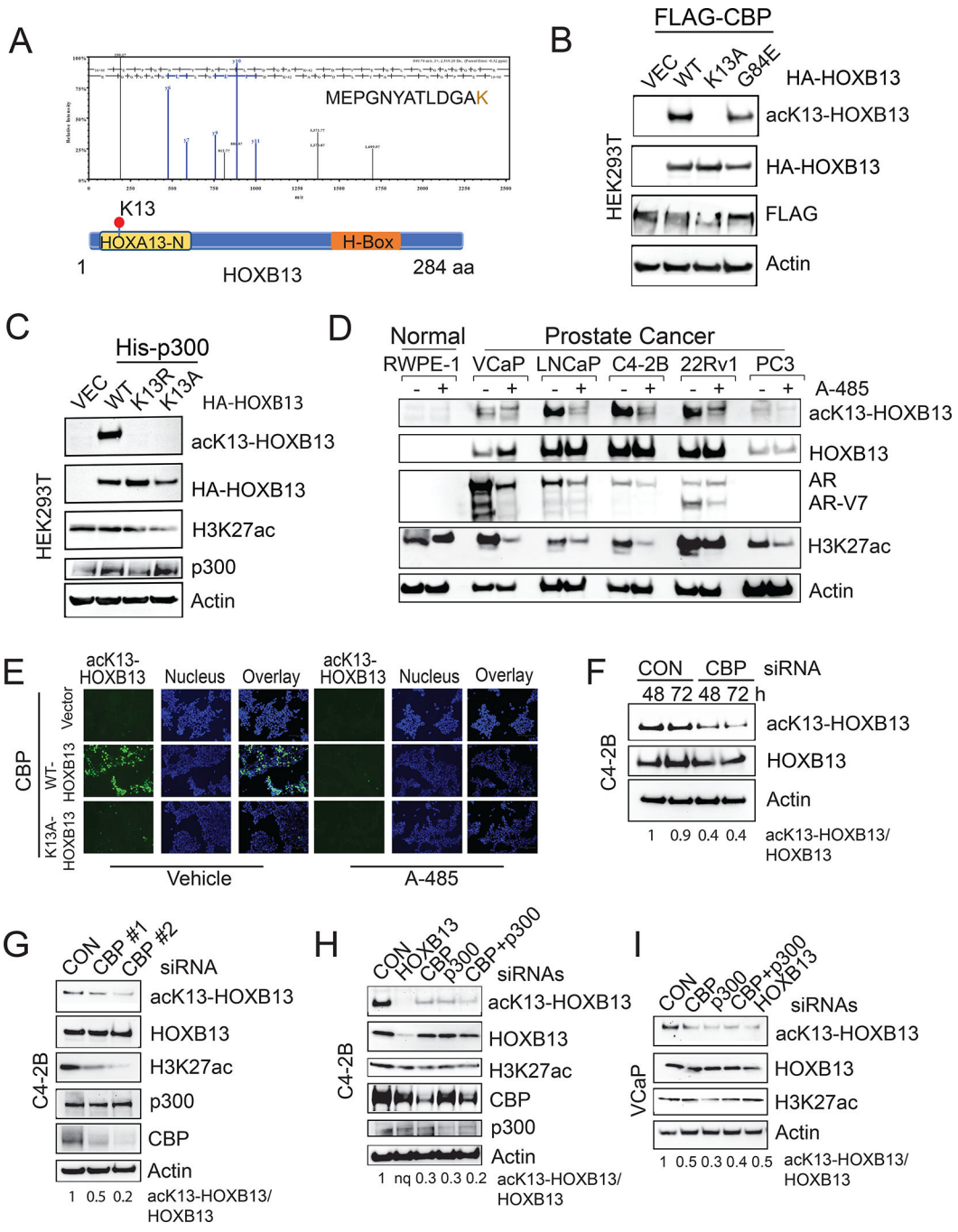

Figure 1. HOXB13 is acetylated by p300/CBP at a highly conserved Lys (K) 13 residue.

A, Mass spectrometry analysis of immunoaffinity-purified HOXB13. A peptide corresponding to acetylated HOXB13-K13 was detected with a mass-to-charge ratio of 840.74 m/z and molecular weight of 2519.20 Da. Schematic shows the K13 acetylation site at the N-terminus and the DNA binding homeobox domain (216 to 275 aa) of HOXB13. **B,** HA-tagged WT HOXB13, or HOXB13K13A, or HOXB13G84E mutants were co-expressed with FLAG-tagged CBP in HEK293T cells. Immunoblot analysis with acK13-HOXB13, HA, FLAG tag and Actin antibodies. **C,** HA-tagged wild type (WT)

Author Manuscript Author Manuscript Author Manuscript Author Manuscript

HOXB13, HOXB13K13A or HOXB13K13R were co-expressed with His-tagged p300 in HEK293T cells. Immunoblot analysis for acK13-HOXB13, HOXB13, H3K27ac, Histidine or Actin. **D,** Immunoblot analysis of acK13-HOXB13, pan-HOXB13, AR, H3K27ac, and actin in normal and PC cell lines treated with Vehicle or A-485 (5μM). Actin is used as a normalization control. **E**, Immunofluorescence analysis with anti-acK13-HOXB13 antibody and DAPI nuclear stain; merged image (overlay) is shown. Scale bars are 200 μm. **F,** C4-2B cells transfected with control or CBP specific siRNAs and cultured for 48 and 72 hrs. Immunoblot analysis with indicated antibodies. **G,** C4-2B cells transfected with control, and two different CBP specific siRNAs and harvested after 48 hrs. Immunoblot analysis with indicated antibodies. **H,** C4-2B cells transfected with control, HOXB13, p300, and/or CBP specific siRNAs and cultured for 48 hrs. Immunoblot analysis with indicated antibodies. **I,** VCaP cells transfected with control, HOXB13, p300, and/or CBP specific siRNAs and cultured for 48 hrs. Immunoblot analysis with indicated antibodies. Quantitation of the ratio of acK13-HOXB13/pan-HOXB13 is shown in **F-I.** nq: not quantified.

Author Manuscript
Author Manuscript
Author Manuscript
Author Manuscript

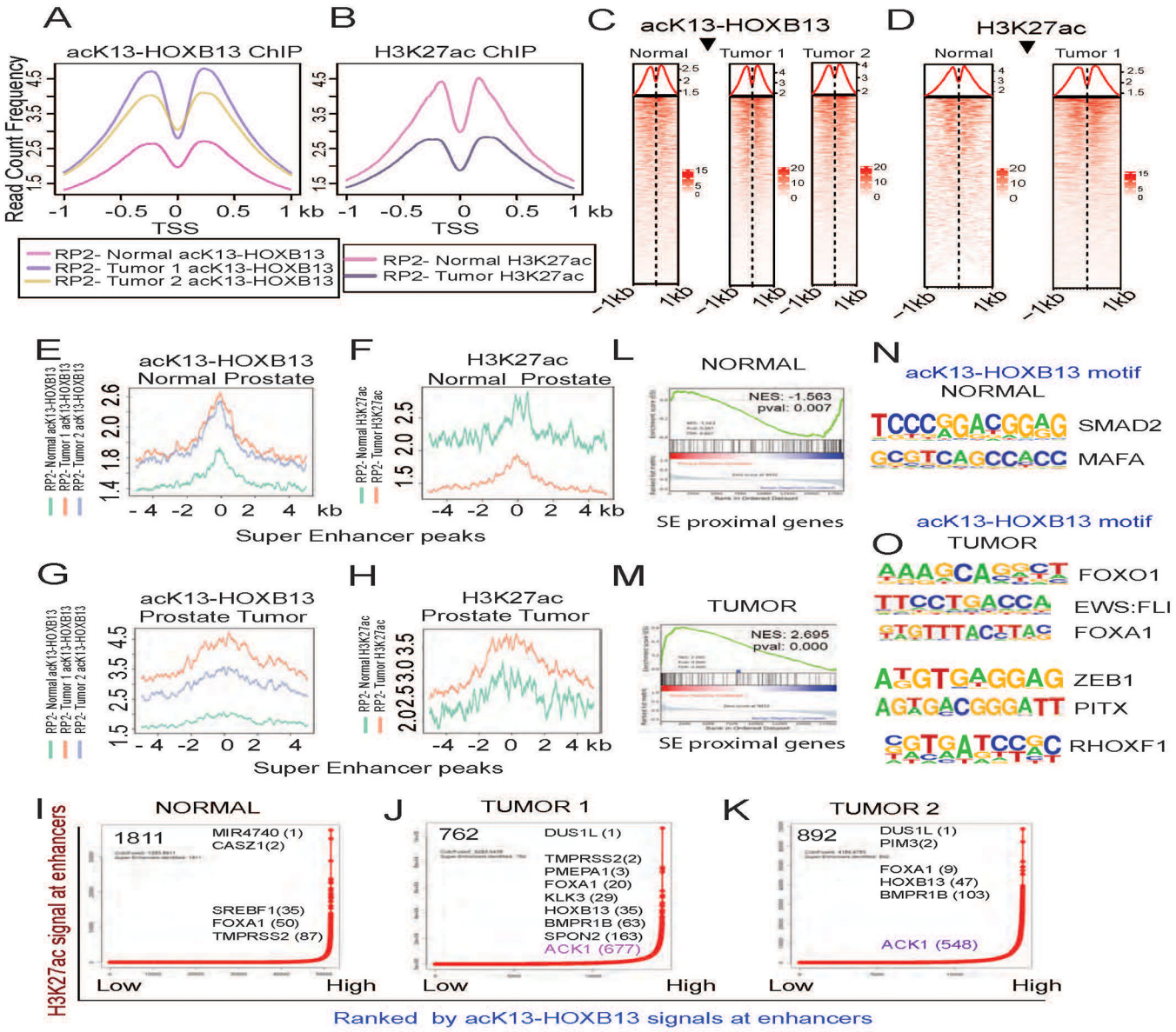

Figure 2. acK13-HOXB13 genome-wide binding enrichment in human primary prostate tumors.

A, ChIP profile of acK13-HOXB13 binding in human normal (pink) and prostate tumor #1 (purple) and prostate tumor #2 (mustard) within 1 kb of the TSSs. **B,** ChIP profile of H3K27ac in human normal prostate (pink) and tumor #1 (purple) within 1 kb of the TSSs. **C,** Heatmap of acK13-HOXB13 binding peaks within 1 kb of TSSs in prostate normal and tumor. **D,** Heatmap of H3K27ac peaks within 1 kb of TSSs in prostate normal and tumor. **E,** ChIP peak profile of acK13-HOXB13 and **F,** H3K27ac signals in normal prostates. **G**, ChIP peak profile of acK13-HOXB13 binding in prostate tumor #1 and tumor #2 and; **H,** H3K27ac in prostate tumor #1 within 4 kb of characterized SEs. **I-K,** ROSE in matched normal and two spatially distinct tumor specimens from a PC patient (age 51 years) who underwent a radical prostatectomy. **L,** acK13-HOXB13-enriched SE proximal in normal prostate (top panel; NES = −1.563, FDR q = 0.007) and **M,** Prostate Tumor (bottom panel;

NES = 2.695, FDR *q*=0.000). Homer *de novo* motifs analysis of acK13-HOXB13 binding sites in normal prostate; **N**, and prostate tumor, **O**.

Author Manuscript Author Manuscript Author Manuscript Author Manuscript

Author Manuscript Author Manuscript Author Manuscript Author Manuscript

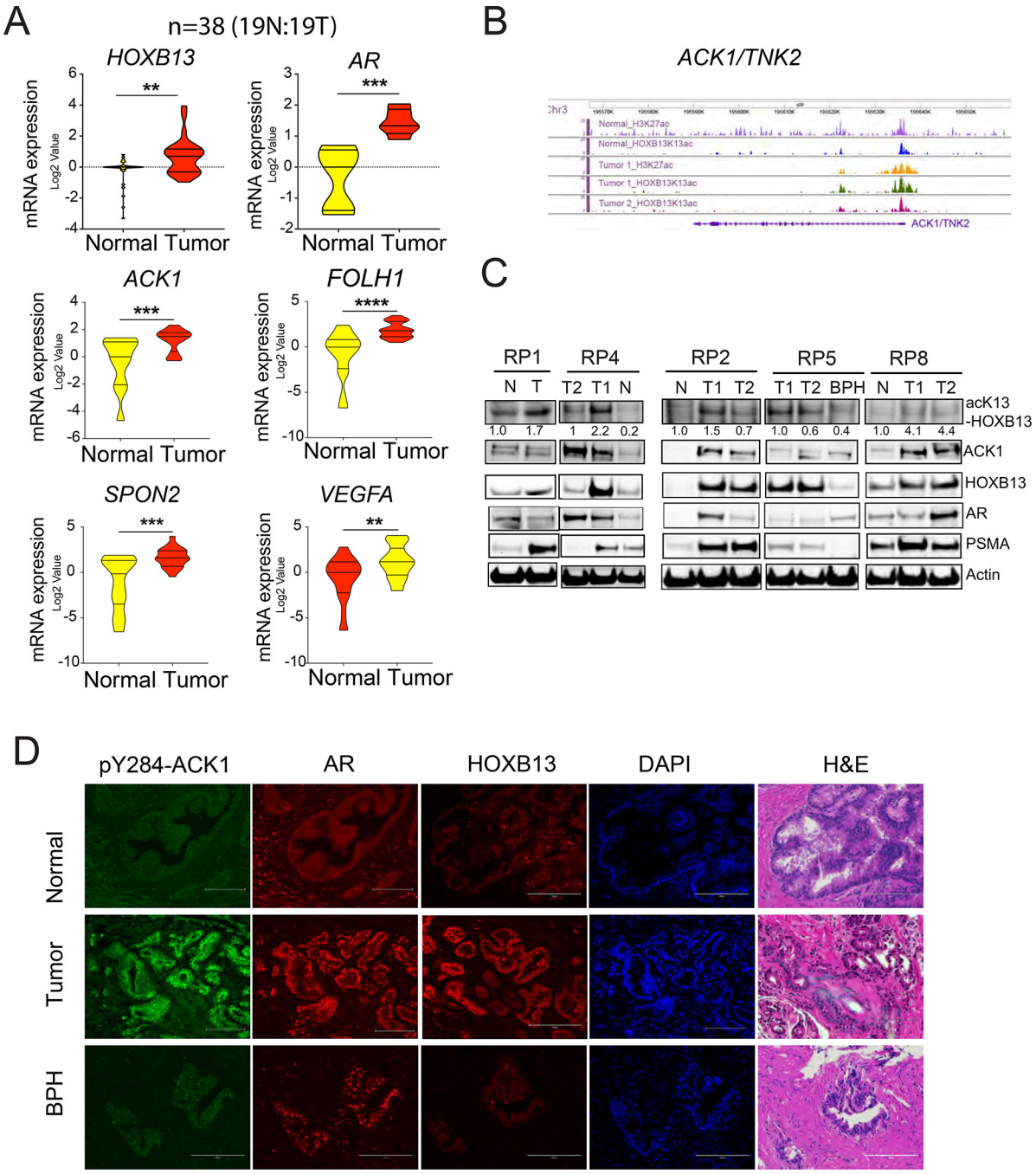

Figure 3. Expression analysis of acK13-HOXB13 regulated targets in primary prostate cancer.

A, qRT-PCR of acK13-HOXB13 target genes in normal (N) and tumor (T) tissues after RP; Gene expression normalized to actin; ****p<0.0001, ***p<0.001, **p<0.01 (n = 19N and 19T matched specimens: total 38). **B,** Genome browser view of acK13-HOXB13 and H3K27ac binding at the *ACK1* gene locus in the patient specimens after radical prostatectomy (RP). **C,** Immunoblot analysis of acK13-HOXB13, ACK1, pan-HOXB13, AR, and PSMA in patient specimens; normal (N), PC (T), and benign prostatic hyperplasia (BPH). Actin is a normalization control. Quantitation of acK13-HOXB13 signal in tumors

relative to normal. **D,** Immunofluorescent staining for pY284-ACK1, AR, HOXB13 and DAPI-nucleus (blue) in FFPE specimens. Hematoxylin and Eosin Staining (Last panel). Scale bar =100 μm.

Author Manuscript Author Manuscript Author Manuscript Author Manuscript

Author Manuscript Author Manuscript Author Manuscript Author Manuscript

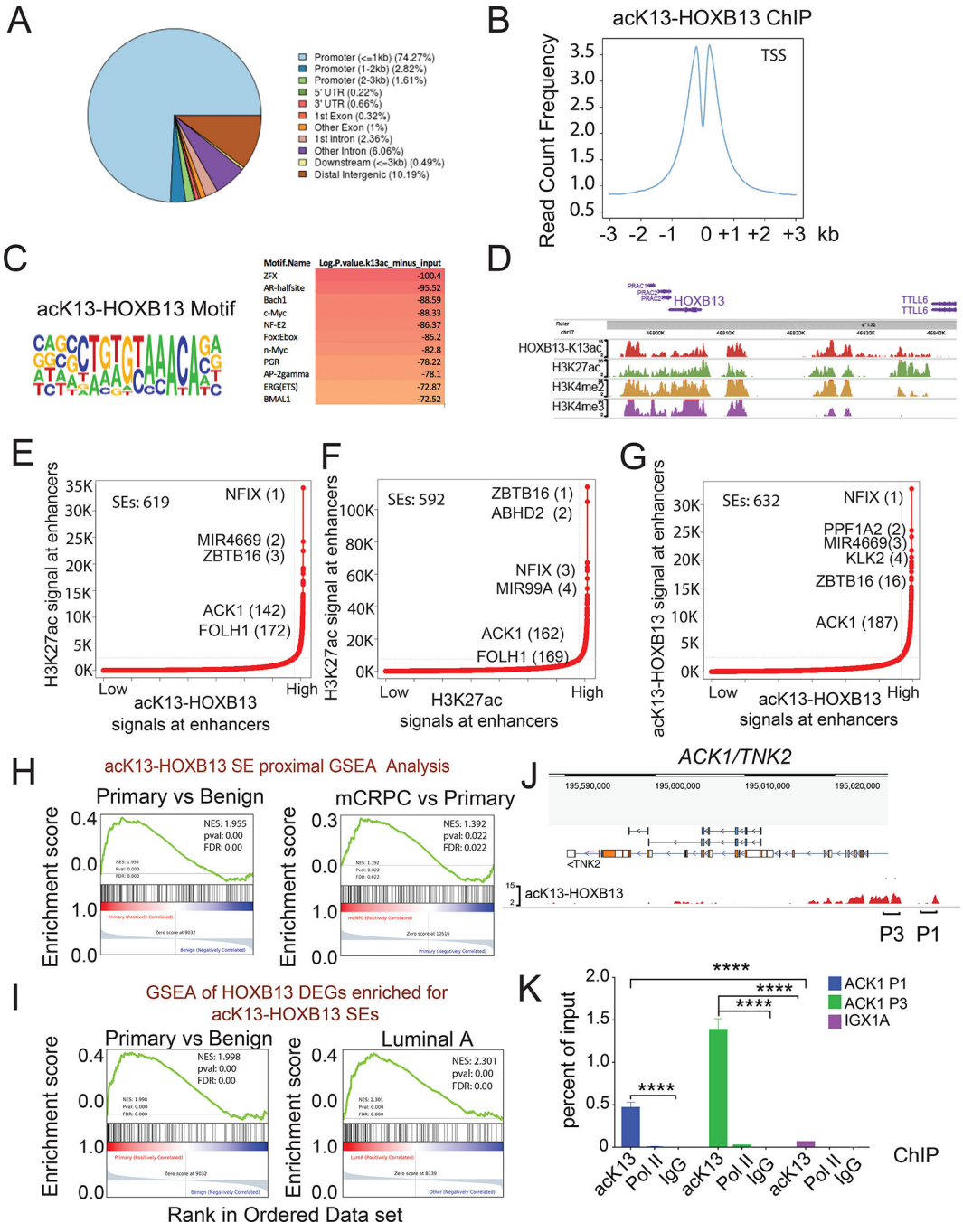

Figure 4. acK13-HOXB13 marks super enhancers of CRPC target genes.

A, Cross-linked chromatin extracts from androgen-deprived C4-2B were immunoprecipitated with acK13-HOXB13 or IgG. The pie-chart shows the distribution of acK13-HOXB13 genome-wide signals. **B,** Binding profile of acK13-HOXB13 −/+ 3 kb of the TSS. **C,** acK13-HOXB13 binding is enriched for GTAAACA motifs. The other top binding motifs are shown in the table. **D,** Genome browser view of acK13-HOXB13 peaks at *HOXB13* (top panel) in C4-2B CRPCs. Peaks were normalized to input or control IgG. H3K27ac, H3K4me2, and H3K4me3 peaks correspond to ChIP-sequencing data from

Author Manuscript Author Manuscript Author Manuscript Author Manuscript

C4-2B (GSE72714). **E-G,** ROSE analysis enrichment for selection of acK13-HOXB13 peak-enriched SEs. **H,** GSEA of acK13-HOXB13 signal marked SE proximal genes in mCRPCs relative to primary PCs (NES = 1.392; FDR $q = 0.022$) and in primary PC relative to normal (NES= 1.955; FDR $q=0.000$). **I,** Integrative GSEA analysis of HOXB13 DEGs proximal to acK13-HOXB13 signal SEs. Left panel: NES = 1.998; FDR $q = 0.000$. Right panel: NES = 2.301; FDR $q = 0.000$). **J,** acK13-HOXB13 tracks at the *ACK1/TNK2* genomic locus (>chr3:195635389–195636094; peaks 1 [P1] and 3 [P3]). **K,** Direct ChIP-qPCR of acK13-HOXB13, RNA Pol II or IgG at the *ACK1* locus in C4-2B cells; n = 3 technical replicates. *IGX1A*, control for non-specific binding; ****$p<0.0001$ (one-way ANOVA). Data are represented as mean ± SEM. Data are representative of two independent biological replicates.

Author Manuscript Author Manuscript Author Manuscript Author Manuscript

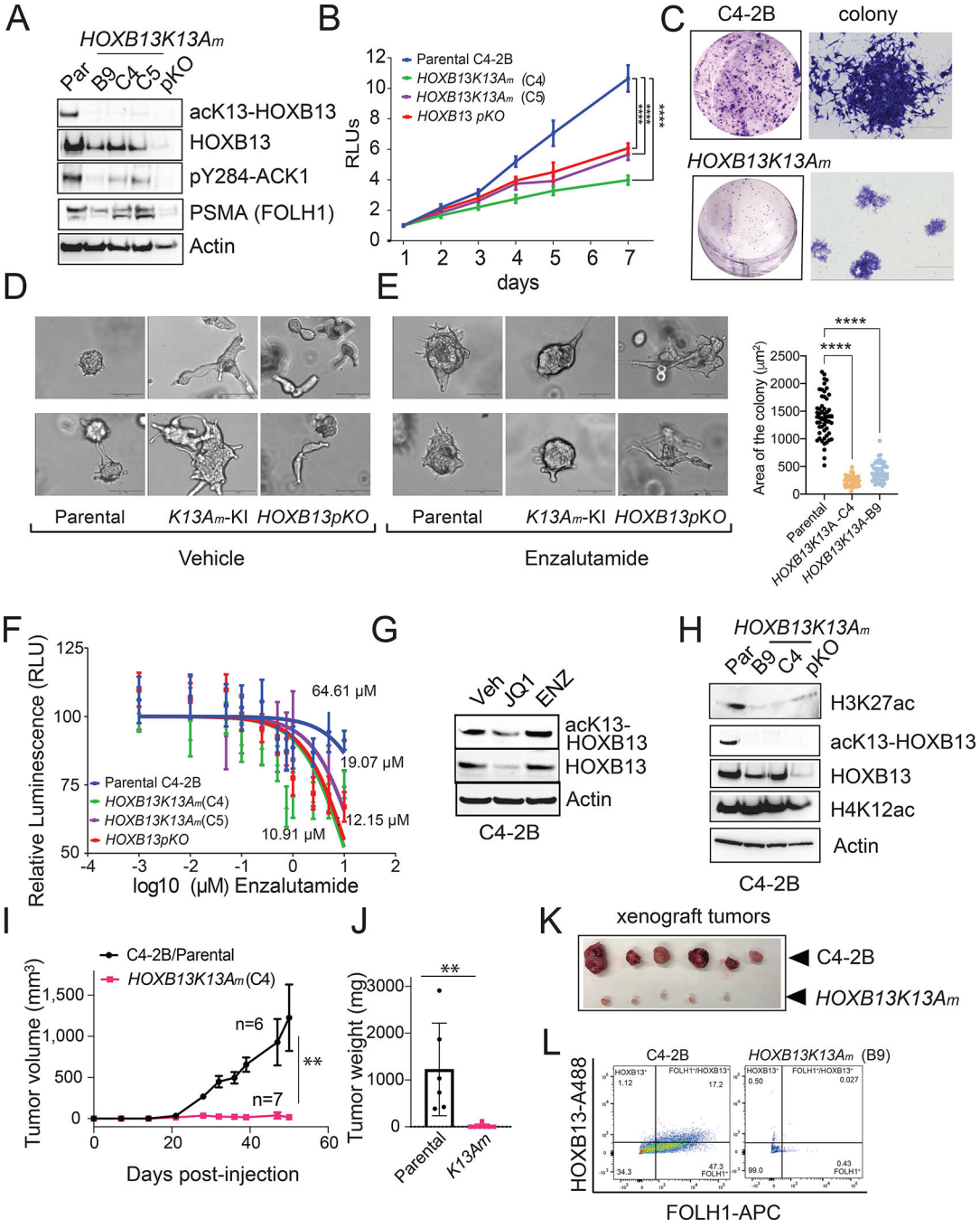

Figure 5. acK13-HOXB13 regulates self-renewal, prostate tumor growth and Enzalutamide resistance of mCRPC.

A, Immunoblot analysis with indicated antibodies in parental, *HOXB13K13A* mutant (KI, clones B9, C4 and C5), and *HOXB13pKO* C4-2B cells. **B,** Cell proliferation assay with isogenic parental C4-2B and *HOXB13pKO* and *HOXB13K13A* mutant clones. ****p<0.0001 (one-way ANOVA). **C,** C4-2B and *HOXB13K13A* mutant in colony formation assay visualized by crystal violet staining. n=6 replicates. Scale bar 300 μm. Scatter plot of colonies shown in lower panel (n ~50 colonies; area of each colony

Author Manuscript Author Manuscript Author Manuscript Author Manuscript

on Y axis). ****p<0.0001 (one-way ANOVA). **D-E,** Spheroid assay: C4-2B parental, *HOXB13K13A* and *HOXB13pKO* cells treated with vehicle (DMSO) alone (D) or (E) ENZ (1 μM). Scale bars represent 100 μm. **F,** Parental C4-2B, *HOXB13pKO,* and *HOXB13K13A* (C4 and C5) cells treated with ENZ for 96h. IC_{50} was determined by Cell titer-Glo assay (n = 8 replicates per condition). **G,** Immunoblot analysis of acK13-HOXB13 and HOXB13 in C4-2B cells treated with either the BET inhibitor, JQ1, or ENZ (5 μM) for 48 hours. (n=2; representative of biological replicates). **H,** Immunoblot analysis of with indicated antibodies in C4-2B parental, *HOXB13K13A* (B9 and C4 clones), and *HOXB13pKO* cells. **I,** Male SCID mice were implanted with isogenic parental C4-2B (n = 6) or the *HOXB13K13A* mutant cell lines (n = 7); Data are presented as mean ± SEM; **p < 0.0076 (unpaired two-tailed Student's t-test). **J,** Tumor weights from (J) at the completion of 7 weeks after injection; Data are presented as mean ± SEM; **p < 0.0083 (unpaired Student's t-test)**. K,** Post-harvest xenograft tumor images of isogenic C4-2B parental or *HOXB13K13A* C4 clone (n=6 or 7). **L,** Flow cytometry analysis of HOXB13-Alexa 488 and FOLH1-APC expression in isogenic C4-2B parental or *HOXB13K13A* xenograft tumors (n=3 in each condition). Actin is used as the normalization control for all immunoblots.

Author Manuscript Author Manuscript Author Manuscript Author Manuscript

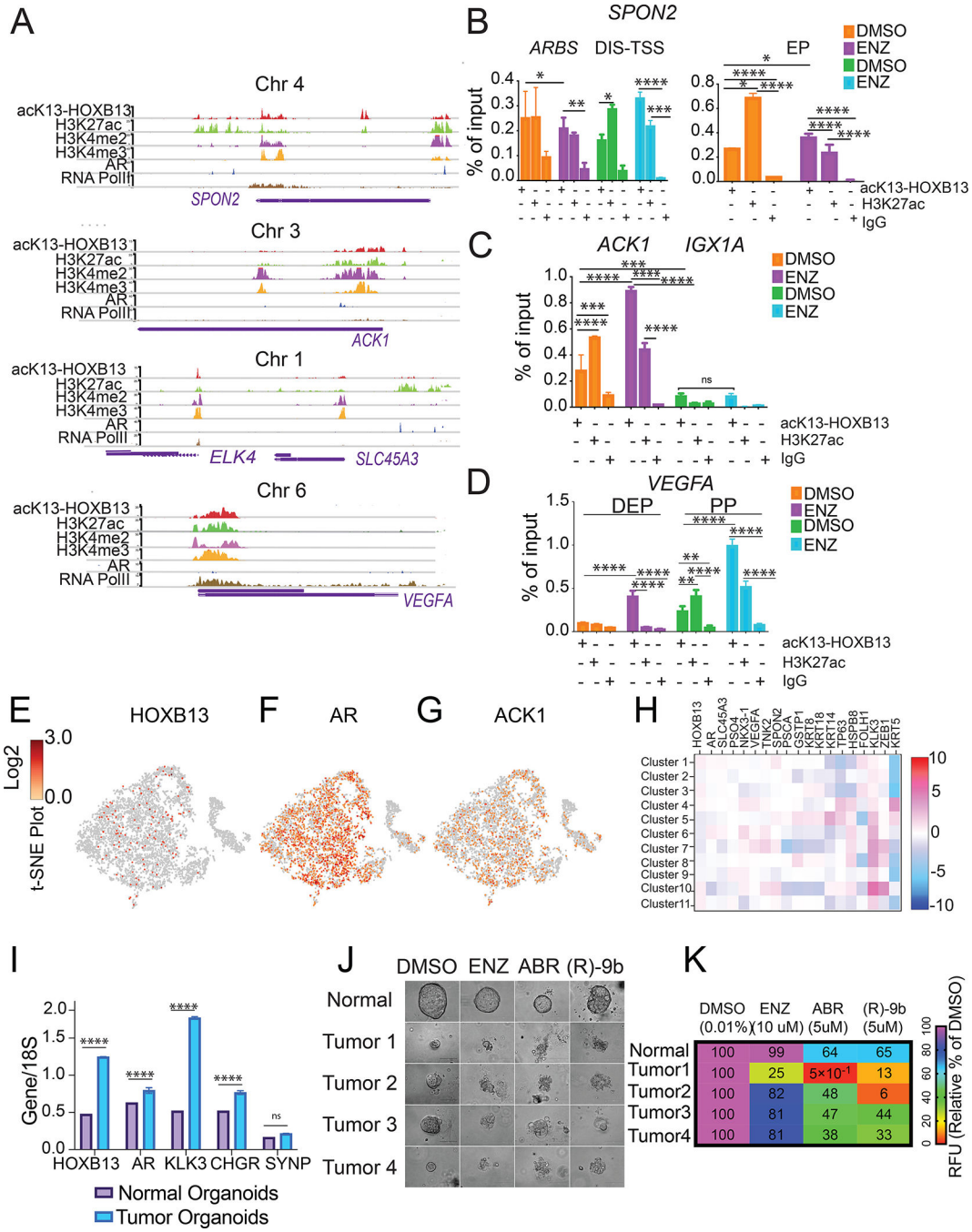

Figure 6. acK13-HOXB13-is recruited to super enhancers despite androgen deprivation.

A, Genome browser view of acK13-HOXB13, H3K27ac, H3K4me2, H3K4me3, RNA Pol II, and AR binding at *SPON2*, *ACK1, SLC45A3/Prostein*, and *VEGFA* in C4-2B. **B-D,** ChIP-qPCR to detect acK13-HOXB13 and H3K27ac binding at the **B**, *SPON2* **C**, *ACK1* and *IGX1A* - control and **D**, *VEGFA* genes in C4-2B treated with vehicle alone (DMSO) or ENZ (5 μM). EP, Enhancer primer. ARBS AR binding site; DIS-TSS Distal to TSS. DEP, Distal Enhancer; PP, Proximal Enhancer. n = 3 technical replicates, ****$p < 0.0001$, ns = not significant (one-way ANOVA). **E-G,** t-distributed stochastic neighbor embedding

Author Manuscript Author Manuscript Author Manuscript Author Manuscript

(t-SNE) analysis of single-cell RNA sequencing data of normal human prostate organoid cultured for 14 days (HOXB13, AR and ACK1 expression in individual clusters is shown). **H**, Heatmap of cell-lineage specific markers and ACK1(TNK2) is shown. **I,** qRT-PCR for PC marker expression in Normal (N) and tumor (T) PDOs (n=4 each). ****$p < 0.0001$, ns = not significant (one-way ANOVA). **J**, Organoids were cultured in the presence of the vehicle, (R)-9b, or anti-androgens ENZ or abiraterone. Phase-contrast microscopy images are as shown; scale bar 50 μm. **K**, Normal (N) and tumor (T) PDOs were treated with anti-androgens or ACK1 inhibitor (R)-9b. Viability was measured with Cell-titer Glo assays of organoid lysates. Data are mean ± SEM.